Shell-model calculations of stellar weak interaction rates:
II. Weak rates for nuclei in the mass range $A = 45 - 65$ in supernovae environment

K. Langanke and G. Martínez-Pinedo

Institut for Fysik og Astronomi, Århus Universitet, DK-8000 Århus C, Denmark

(February 8, 2008)

Based on large-scale shell model calculations we have determined the electron capture, positron capture and beta-decay rates on more than 100 nuclei in the mass range $A = 45$-65. The rates are given for densities $\rho Y_e = 10^7$-10^{10} mol/cm^3 and temperatures $T = 10^9$-10^{10} K and hence are relevant for both types of supernovae (Type Ia and Type II). The shell model electron capture rates are significantly smaller than currently assumed. For proton-to-baryon ratios $Y_e = 0.42$-0.46 mol/g, the beta-decay rates are faster than the electron capture rates during the core collapse of a massive star.

I. INTRODUCTION

Astrophysical environments can reach very high densities and temperatures. Under these conditions (temperatures T larger than a few 10^9 K), reactions mediated by the strong and electromagnetic force are in chemical equilibrium and the matter composition is given by nuclear statistical equilibrium [1,2], i.e. it is determined mainly due to the nuclear binding energies subject to the constraint that the total number of protons in the composition balances the number of electrons present in the environment. Introducing the electron-to-baryon ratio Y_e (units of mol/g), this constraint can be formulated as

$$\sum_k \frac{Z_k}{A_k} X_k = Y_e; \quad \sum_k X_k = 1 \qquad (1)$$

where the sum is over all nuclear species present and Z_k, A_k, and X_k are the proton number, mass number and mass fraction of species k, respectively. Importantly, in these astrophysical environments the relevant density and time scales are often such that the neutrinos are radiated away, so that reactions mediated by the weak interaction are not in equilibrium. Thus, weak interaction rates play a decisive role in these environments changing Y_e and hence the composition of the matter.

Among these astrophysical environments are the two major contributors to the element production in the universe: supernovae of type Ia and type II (e.g. [3]). A type Ia supernova is usually associated with a thermonuclear explosion on an accreting white dwarf. Hydrogen mass flow from the companion star in the binary system at rather high rates leads to steady hydrogen and helium burning on the surface, increasing the carbon and oxygen mass of the white dwarf. Finally carbon is ignited in the center of the star leading to a thermonuclear runaway. A burning front then moves outwards through the star at subsonic speed, finally leading to a detonation which explodes the star. Several issues (including the masses of the stars in the binary, the mass accretion history and composition, the matter transport during the explosion, the speed of the burning front) are currently still under

debate (e.g. [4]). It appears, however, established that electron capture will occur in the burning front driving the matter to larger neutron excess. As the observed iron in the universe is made roughly in equal amounts by type Ia and type II supernovae, type Ia supernovae should produce the relative abundances within isotope chains in the iron mass region in agreement within a factor of 2 with the observed solar abundances [5]. Provided the electron capture rates are sufficiently well known (matter is in nuclear statistical equilibrium inside a type Ia supernova), this requirement allows to put severe constraints on type Ia supernova models [6].

A type II supernova is related to the core collapse of a massive star. Here the core of a massive star becomes dynamically unstable when it exhausts its nuclear fuel. If the core mass exceeds the appropriate Chandrasekhar mass, electron degeneracy pressure cannot longer stabilize its center and it collapses. In the initial stage of the collapse, electrons are captured by nuclei in the nickel mass range, thus reducing Y_e. Associated is a decrease in degeneracy pressure and energy, as the neutrinos can still leave the star; both effects accelerate the collapse. With decreasing Y_e, i.e. with increasing neutron excess of the nuclei present, β decay becomes more important and can compete with electron capture.

Under the stellar conditions discussed above, the weak interaction rates are dominated by Gamow-Teller (GT) and, if applicable, by Fermi transitions. Bethe *et al.* [7] recognized the importance of the collective GT resonance for stellar electron capture. Shortly after, Fuller, Fowler and Newman (usually abbreviated as FFN [8–11]) estimated the stellar electron capture and beta-decay rates systematically for nuclei in the mass range $A = 45 - 60$ considering two distinct contributions. At first, these authors estimated the GT contributions to the rates by a parametrization based on the independent particle model. The rate estimate has then been completed by including Fermi transitions and by experimental data for discrete transitions, whenever available. Unmeasured allowed GT transitions have been assigned an empirical value ($\log ft = 5$). One of the important ideas in the seminal work by FFN was to recognize the role played by the

GT resonance in β^- decay via the GT back resonance in the parent nucleus (the GT back resonance are the states reached by the strong GT transitions in the inverse process (electron capture) built on the ground and excited states, see [9,10]) allowing for a transition with a large nuclear matrix element and increased phase space. Until now the FFN weak interaction rates are key ingredients in supernova simulations.

The general formalism to calculate weak interaction rates for stellar environment has been already given by Fuller *et al.* [8–11]. What had not been possible at the time when FFN did their pioneering work was to solve the associated nuclear structure problem with the necessary accuracy and predictive power. Several years ago, Aufderheide, Mathews and collaborators [12–14] pointed out that the interacting shell model is the method of choice for this job. In fact, using the newly developed shell model Monte Carlo techniques [15,16] electron capture rates for selected nuclei have been derived [17], but it became apparent that shell model diagonalization calculations are preferable [18,19] as they allow for detailed spectroscopy and do not have restrictions in their applicability to odd-odd and odd-A nuclei as the shell model Monte Carlo method has at low temperatures [16]. Before calculating weak interaction rates for a large set of nuclei in the $A = 45$-65 mass region, it had to be proven that state-of-the-art shell model diagonalization is indeed capable of reliably solving the required nuclear structure problems. This proof has been given in Ref. [20]. This paper reported about large-scale shell model calculations covering the relevant mass range. The studies were performed at a truncation level in the pf shell at which the GT strength distributions are virtually converged. As residual interaction a slightly modified version of the wellknown KB3 interaction [21] has been used; the slight modifications correct for the small overbinding at the $N = 28$ shell closure encountered with the original KB3 force [20]. In general, it has been demonstrated that the shell model reproduces all measured GT_+ distributions very well and gives a very reasonable account of the experimentally known GT_- distributions. Further, the lifetimes of the nuclei and the spectroscopy at low energies is simultaneously also described well. Ref. [20] has therefore shown that modern shell model approaches have the necessary predictive power to reliably estimate stellar weak interaction rates.

In this paper we will use the shell model approach of [20] and derive the weak interaction rates for more than 100 nuclei in the mass range $A = 45$-65 at a temperature and density regime relevant for supernova applications. Our paper is organized as follows. In section 2 we will repeat the derivation of the necessary formalism for the weak rates. The results are presented and explored in section 3. In this section we will also compare them to the pioneering work of FFN. In this comparison we will find systematic differences. The origin for these differences will be explored and discussed in section 4.

II. STELLAR WEAK INTERACTION RATES FORMALISM

The definition of the stellar electron and positron capture and β-decay rates has been derived by Fuller, Fowler and Newman [8–11]. We will here repeat the formulae and ideas which will allow us to explain our strategy and procedure to calculate these rates and to point out differences with previous compilations.

A. General formalism

We computed rates for four processes mediated by the charged weak interaction:

1. Electron capture (ec),

$$(Z, A) + e^- \rightarrow (Z - 1, A) + \nu. \qquad (2a)$$

2. β^+ decay (β^+),

$$(Z, A) \rightarrow (Z - 1, A) + e^+ + \nu. \qquad (2b)$$

3. Positron capture (pc),

$$(Z, A) + e^+ \rightarrow (Z + 1, A) + \bar{\nu}. \qquad (2c)$$

4. β^- decay (β^-),

$$(Z, A) \rightarrow (Z + 1, A) + e^- + \bar{\nu}. \qquad (2d)$$

The rate for these weak processes is given by

$$\lambda^\alpha = \frac{\ln 2}{K} \sum_i \frac{(2J_i + 1)e^{-E_i/(kT)}}{G(Z, A, T)} \sum_j B_{ij}\Phi_{ij}^\alpha, \qquad (3)$$

where the sums in i and j run over states in the parent and daugther nuclei respectively and the superscript α stands for ec, β^+, pc or β^-. The constant K is defined as

$$K = \frac{2\pi^3(\ln 2)\hbar^7}{G_F^2 V_{ud}^2 g_V^2 m_e^5 c^4}, \qquad (4)$$

where G_F is the Fermi coupling constant, V_{ud} is the up-down element in the Cabibbo-Kobayashi-Maskawa quark-mixing matrix and $g_V = 1$ is the weak vector coupling constant. K can be determined from superallowed Fermi transitions and we used $K = 6146 \pm 6$ s [22]. $G(Z, A, T) = \sum_i \exp(-E_i/(kT))$ is the partition function of the parent nucleus. B_{ij} is the reduced transition probability of the nuclear transition. We will only consider Fermi and GT contributions which, however, has been shown to be quite sufficient:

$$B_{ij} = B_{ij}(F) + B_{ij}(GT). \qquad (5)$$

2

The GT matrix is given by:

$$B_{ij}(GT) = \left(\frac{g_A}{g_V}\right)^2_{\text{eff}} \frac{\langle j||\sum_k \boldsymbol{\sigma}^k \boldsymbol{t}_\pm^k||i\rangle^2}{2J_i+1}, \qquad (6)$$

where the matrix element is reduced with respect to the spin operator $\boldsymbol{\sigma}$ only (Racah convention [23]) and the sum runs over all nucleons. For the isospin rising and lowering operators, $\boldsymbol{t}_\pm = (\boldsymbol{\tau}_x \pm i\boldsymbol{\tau}_y)/2$, we use the convention $\boldsymbol{t}_+ p = n$; thus, '+' refers to electron capture and β^+ transitions and '−' to positron capture and β^- transitions. Finally, $(g_A/g_V)_{\text{eff}}$ is the effective ratio of axial and vector coupling constants that takes into account the observed quenching of the GT strength [24]. We use [25–27]

$$\left(\frac{g_A}{g_V}\right)_{\text{eff}} = 0.74 \left(\frac{g_A}{g_V}\right)_{\text{bare}}, \qquad (7)$$

with $(g_A/g_V)_{\text{bare}} = -1.2599(25)$ [22]. If the parent nucleus (with isospin T) has a neutron excess, then the GT$_-$ operator can connect to states with isospin $T-1$, T, $T+1$ in the daughter, while GT$_+$ can only reach states with $T+1$. This isospin selection is one reason why the GT$_+$ strength is more concentrated in the daughter nucleus (usually within a few MeV around the centroid of the GT resonance), while the GT$_-$ is spread over 10-15 MeV in the daughter nucleus and is significantly more structured.

The Fermi matrix element is given by:

$$B_{ij}(F) = \frac{\langle j||\sum_k \boldsymbol{t}_\pm^k||i\rangle^2}{2J_i+1}. \qquad (8)$$

In our calculations isospin is a good quantum number and the Fermi transition strength is concentrated in the isobaric analog state (IAS) of the parent state. Equation (8) reduces to,

$$B_{ij}(F) = T(T+1) - T_{z_i}T_{z_j}, \qquad (9)$$

where j denotes the IAS of the state i. We neglect the reduction in the overlap between nuclear wave functions due to isospin mixing which is estimated to be small ($\approx$ 0.5% [22]).

The last factor in equation (3), Φ_{ij}^α, is the phase space integral given by

$$\Phi_{ij}^{ec} = \int_{w_l}^\infty wp(Q_{ij}+w)^2 F(Z,w)$$
$$S_e(w)(1 - S_\nu(Q_{ij}+w))dw, \qquad (10a)$$

$$\Phi_{ij}^{\beta^+} = \int_1^{Q_{ij}} wp(Q_{ij}-w)^2 F(-Z+1,w)$$
$$(1 - S_p(w))(1 - S_\nu(Q_{ij}-w))dw, \qquad (10b)$$

$$\Phi_{ij}^{\beta^-} = \int_1^{Q_{ij}} wp(Q_{ij}-w)^2 F(Z+1,w)$$
$$(1 - S_e(w))(1 - S_\nu(Q_{ij}-w))dw, \qquad (10c)$$

$$\Phi_{ij}^{pc} = \int_{w_l}^\infty wp(Q_{ij}+w)^2 F(-Z,w)$$
$$S_p(w)(1 - S_\nu(Q_{ij}+w))dw, \qquad (10d)$$

where w is the total, rest mass and kinetic, energy of the electron or positron in units of $m_e c^2$, and $p = \sqrt{w^2-1}$ is the momentum in units of $m_e c$. We have introduced the total energy available in β-decay, Q_{ij}, in units of $m_e c^2$

$$Q_{ij} = \frac{1}{m_e c^2}(M_p - M_d + E_i - E_j), \qquad (11)$$

where M_p, M_d are the nuclear masses of the parent and daughter nucleus, respectively, while E_i, E_j are the excitation energies of the initial and final states. We have calculated the nuclear masses from the tabulated atomic masses neglecting atomic binging energies. w_l is the capture threshold total energy, rest plus kinetic, in units of $m_e c^2$ for positron (or electron) capture. Depending on the value of Q_{ij} in the corresponding electron (or positron) emission one has $w_l = 1$ if $Q_{ij} > -1$, or $w_l = |Q_{ij}|$ if $Q_{ij} < -1$. S_e, S_p, and S_ν are the positron, electron, and neutrino (or antineutrino) distribution functions, respectively. For the stellar conditions we are interested in, electrons and positrons are well described by Fermi-Dirac distributions, with temperature T and chemical potential μ. For electrons,

$$S_e = \frac{1}{\exp\left(\frac{E_e - \mu_e}{kT}\right) + 1}, \qquad (12)$$

with $E_e = wm_e c^2$. The positron distribution is defined similarly with $\mu_p = -\mu_e$. The chemical potential, μ_e, is determined from the density inverting the relation

$$\rho Y_e = \frac{1}{\pi^2 N_A}\left(\frac{m_e c}{\hbar}\right)^3 \int_0^\infty (S_e - S_p)p^2 dp, \qquad (13)$$

where N_A is Avagadro's number. Note that the density of electron-positron pairs has been removed in (13) by forming the difference $S_e - S_p$.

In supernovae weak interactions with nuclei with mass numbers $A = 45$-65 occur at such densities that the neutrinos can leave the star unhindered. Thus, there is no neutrino blocking of the phase space, i.e. $S_\nu = 0$.

The remaining factor appearing in the phase space integrals is the Fermi function, $F(Z,w)$, that corrects the phase space integral for the Coulomb distortion of the electron or positron wave function near the nucleus. It can be approximated by

$$F(Z,w) = 2(1+\gamma)(2pR)^{-2(1-\gamma)}\frac{|\Gamma(\gamma+iy)|^2}{|\Gamma(2\gamma+1)|^2}e^{\pi y}, \qquad (14)$$

where $\gamma = \sqrt{1-(\alpha Z)^2}$, $y = \alpha Zw/p$, α is the fine structure constant, and R is the nuclear radius.

Finally, the calculation of the rates reduces to the evaluation of the nuclear transition matrix elements for the

GT operator. The problem obviously lies in the fact that many states (can) contribute to the two sums over i, j. At first, the finite temperature allows the thermal population of excited states in the parent. Each of these states is then connected to many levels in the daughter nucleus by the GT operators. A state-by-state evaluation of both sums is still beyond present-day computer abilities. Before we summarize our strategy to approximate the sums we recall that previous compilations of the stellar weak rates employed the so-called Brink hypothesis (e.g. [28]): Let $S_0(E)$ be the GT distribution in the daughter nucleus build on the ground state, then it is assumed that the distribution $S_i(E)$ build on the excited state in the parent at excitation energy E_i is the same as S_0, but shifted in energy by E_i, i.e. $S_0(E) = S_i(E + E_i)$. This hypothesis has been tested in various shell model calculations and is found to be valid for the gross structure of the GT distribution. However, it can be badly violated for specific transitions as they occur at low excitation energies (and are important for nuclear lifetimes). This tells us that Brink's hypothesis should not be employed if specific low-lying transitions (which usually exhaust a very small fraction of the total GT strength) dominate the rates or are important. Such situations may occur at low temperatures and densities. When the temperatures and densities are higher so that many states (a few tens or more) contribute, variations in low-lying transition strengths tend to cancel and Brink's hypothesis becomes a valid approximation. We will demonstrate this in detail later in this paper.

B. Evaluation of the rates and checks

Our strategy to calculate the weak rates (2) is best explained by considering a pair of nuclei (Z, A) and $(Z + 1, A)$ connected by the weak processes under discussion here. We have then calculated the GT_+ distributions for all individual levels in the nucleus $(Z + 1, A)$ at modest excitation energies and the GT_- strength distributions for the low-lying levels in the nucleus (Z, A). Whenever experimental information about excitation energies or GT transition strengths is available, the shell model results have been replaced by data. Otherwise the shell model predictions are used. The quality of these calculations is demonstrated in [20] where calculated spectra and lifetimes are compared to data. For even-even parents we considered explicitly the lowest 0^+, 4^+ and the two lowest 2^+ levels which describe the spectrum typically upto excitation energies of 2 MeV. Depending on the level spectrum, we adopted between 4 and 12 individual states for odd-A and odd-odd parent nuclei including at least the shell model spectrum at excitation energies below 1 MeV explicitly. As our shell model GT distributions have been calculated with 33 Lanczos iterations (see [20]), a state in the parent nucleus is connected to 33 (for angular momenta $J = 0$) til 99 (for angular momenta $J \geq 1$) states in the daughter nucleus by the GT_+ operator, while this magnifold is tripled for the GT_- operator due to the different isospin final states. (However, the T+1 component does not play a role in calculating the rates under the temperature/density conditions we are concerned with and is often omitted.)

While the explicit consideration of the low-lying states guarantees a reliable description of the rates at low temperatures/densities, where individual transitions are often decisive, states at higher excitation energies become increasingly important at the higher temperature and density regimes under consideration here. This is particularly true for the β^- decay rates which is often dominated by the back-resonances under these conditions [9,10]. We have therefore supplemented the contribution of the low-lyin states by the back-resonance contributions which can be derived from the low-lying contributions in the inverse process, i.e. the states populated by electron capture on (β^- decay of) low-lying states became the back-resonances in the β^--decay (electron capture). The back-resonance contribution defined this way does not exhaust the total GT strength built on this excited state. In particular, the capture of high energy electrons in the back-resonance states will lead to states in the daughter which are not included in our model. To correct for these missing transitions we have employed the Brink hypothesis, i.e. we calculate the total GT strength and the centroid E_c for the parent ground state and place the strength of the back-resonance state at an energy $E_i + E_c$, where E_i is the energy of the back-resonance state in the parent.

Fig. 1 illustrates the various contributions to the two sums in the rate formulae. In evaluating these sums we typically consider several hundred states in both the parent and the daughter nucleus. The partition function is consistently derived from the same parent states. We do not introduce a cut-off of levels at the particle separation thresholds [7,29].

To demonstrate the convergence of our rates we will explicitly discuss the pair of nuclei ^{63}Co and ^{63}Ni. Due to Ref. [28], ^{63}Co is among the most important β-decaying nuclei in a presupernova collapse at densities around 10^8 g/cm^3, while electron capture on ^{63}Ni plays a moderate role at the same astrophysical conditions. The Q_β value for this pair of nuclei is 3.672(20) MeV. Thus under laboratory conditions ^{63}Co β-decays to ^{63}Ni, leading dominantly to the excited 5/2 state at 87 keV with an $\log ft$ value of 4.8(1). Our shell model calculation agrees with the data.

Our calculation of the stellar electron capture (and β^+ decay) rate explicitly considers the two lowest $1/2^-$ and $3/2^-$ states and the lowest $5/2^-$ state in ^{63}Ni, which comprises the experimentally known spectrum upto an excitation energy of 1 MeV. Furthermore we include the back-resonances from the inverse reaction which introduces a total of 6 states in the excitation energy interval between 1 and 2 MeV, while experimentally 8 states are known in this energy regime. Between 2 and 5 MeV,
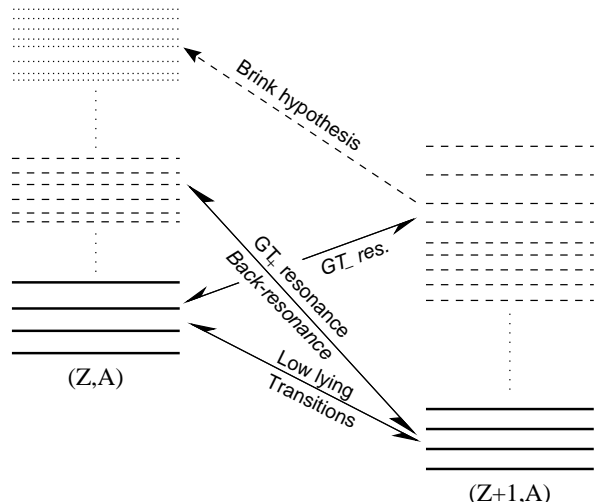
FIG. 1. Sketch of the GT transitions considered in the present estimate of the stellar weak interaction rates. Our evaluation of the sums in Eq. 3 explicitly includes the GT_- and GT_+ strength distributions for the few lowest states in a nucleus. This is supplemented by the back-resonances which are derived from the GT strength distributions of the inverse process, as described in the text. Experimental data for the energies and GT transition strengths have been used, whenever available. Otherwise the shell model results are adopted. Finally the Brink hypothesis (see text) is employed to derive the remaining GT strength and centroid position for back-resonance states. In the sketch these transitions are shown by dashed lines, while the GT transitions, for which either data or shell model results are used, are drawn by solid lines.

we include 16 more states which, however, are probably not fully converged within our Lanczos procedure and thus represent 'averaged GT states' rather than physical states.

Table I demonstrates the convergence of the stellar ^{63}Ni electron capture rate with the number of initial states. We have calculated the rates for various densities between $\rho Y_e = 10^7$ and 10^{10} mol/cm^3. The temperatures have been chosen from the FFN temperature/density grid to be the closest to the expected stellar trajectory in a supernova collapse [28]. The calculations have been performed considering only the ground state, the lowest 2 and 3 states, all 5 states for which shell model GT_+ distributions have been explicitly calculated and finally for our full procedure including individual states and back-resonances.

The calculation performed by restricting the sum over initial states to only the ground state resembles the application of 'Brink's shift hypothesis', as with this assumption the nuclear matrix elements and the phase space factors loose their dependence on the parent state and the sum over initial states cancels the partition function [28]. (We point out that this calculation is, however, not the same as those in Refs. [9,10,28] as we adopt the shell

model GT_+ strength distribution, while the other authors had used an empirical parametrization of the GT strength (see below).) As expected, the application of the Brink hypothesis is not a good approximation at low temperatures and densities where the rate is sensitive to low-lying transitions which can vary strongly between various initial states. The assumption becomes, however, quite acceptable at higher densities where enough high-energy electrons are available to effectively reach the centroid of the GT distribution in the daughter. As stated above, Brink's shift hypothesis works well if centroids are compared. To demonstrate this quantitatively we have calculated the GT centroids (E_{GT}) for the 5 initial states. A measure for the validity of the Brink hypothesis is then given by the difference $E_{GT} - E_x$, where E_x is the shell model excitation energy of the initial state. If measured relative to the ^{63}Ni ground state, this difference is 13.7 MeV for the ground state, while we find 13.7 MeV ($5/2^-$), 13.7 MeV ($3/2^-$), 13.9 MeV (excited $3/2^-$) and 14.1 MeV (excited $1/2^-$) for the other states.

In Table I we also observe that, even at low densities, a convergence is rather fast achieved if the rate comprises a thermal average over a few states.

The ^{63}Co β-decay rate has been calculated by explicitly considering the GT_- distributions for the lowest $7/2^-$ (ground state), $3/2^-$ (at 0.995 MeV), $5/2^-$ (at 1.437 MeV) and $1/2^-$ (at 1.889 MeV) states. Only the $1/2^-$ state has a definitive spin assignment, the spin for the other states has been assigned based on our calculations. These contributions are then supplemented by the back-resonances obtained from the GT_+ distributions of the inverse reaction. These include another 4 states in the excitation energy interval between 1 and 2 MeV and 18 (average) states between 2 and 5 MeV. Due to their construction, the back-resonances have only transitions to the 5 lowest levels in ^{63}Ni. The missing decay channels of these states are, however, significantly suppressed due to the strong Q_β dependence.

In Table II we study the convergence of the ^{63}Co β^- decay rate. The full rate is compared to rates in which the contributions from the 4 individual levels are kept, but the back-resonance contributions are cut at 5 MeV and 3 MeV in the parent nucleus. Additionally we have calculated the rates only from the GT_- distributions of the lowest 4, 2, and 1 states, totally neglecting the back-resonances.

We find that at low temperature/densities the rate can be calculated solely from the individual levels in a good approximation; even the decay rate determined from the ground state alone is already a fair approximation. At moderate and higher densities the back-resonances become increasingly more important. This is easily understood by the fact that at these high densities the Fermi energy of the electrons gets so high that decays from low-lying states are effectively blocked. Correspondingly the β decay rates decrease with increasing density. But we also note from Table II that the rate still converges rather rapidly and that considering the back-resonances upto 5

TABLE I. Convergence of the stellar ^{63}Ni electron capture rate, $\log\lambda^{\rm ec}$, along the stellar trajectory during a supernova collapse (defined by temperature T_9 and density ρ). Our full rate is compared to rates in which only the lowest 5, 3, 2, and 1 states in ^{63}Ni are considered. The 'no Brink' calculation has been performed neglecting those rate contributions which are shown by dashed arrow and are labelled 'Brink hypothesis' in Fig. 1.

T_9	$\log\rho Y_e$	full	no Brink	5 states	3 states	2 states	1 state
3	7	-8.46	-8.46	-8.62	-8.59	-8.46	-9.62
4	8	-5.18	-5.18	-5.29	-5.25	-5.12	-5.83
5	9	-1.74	-1.77	-1.77	-1.72	-1.61	-1.93
7	10	1.78	1.63	1.74	1.78	1.80	1.84

TABLE II. Convergence of the stellar ^{63}Co β^- decay rate, $\log\lambda^{\beta^-}$, along the stellar trajectory during a supernova collapse (defined by temperature T_9 and density ρ_7). Our full rate is compared to rates in which back-resonant states are only considered upto 5 MeV and 3 MeV, respectively, and to rates which are calculated from the GT$_-$ distributions of the lowest 4, 2, and 1 states in ^{63}Co.

T_9	$\log\rho Y_e$	full	cut 5 MeV	cut 3 MeV	4 states	2 states	1 state
3	7	-1.60	-1.60	-1.60	-1.61	-1.62	-1.64
4	8	-1.77	-1.77	-1.79	-1.89	-1.90	-1.97
5	9	-2.55	-2.55	-2.71	-3.52	-3.65	-4.03
7	10	-5.43	-5.51	-5.99	-7.12	-7.30	-7.71

MeV excitation energy gives a sufficient approximation.

We mention that, due to [28], at high densities nuclei in the supernova environment are expected to be more neutron-rich than ^{63}Co. Thus the relevant Q_β values for β decay increase making the final-state blocking by electrons less effective and reducing the importance of back-resonant states relative to the low-lying individual states which we have considered.

III. STELLAR WEAK RATES

We have calculated the stellar weak interaction rates (electron and positron capture, β^- and β^+ decay) for more than 100 nuclei in the mass range $A = 45$-65. The rates have been calculated for the same temperature and density grid as the standard FFN compilations [9,10,30]. An electronic table of our rates is available from the present authors upon request. We have also prepared a table in which the electron capture rates are presented in terms of the 'effective rates' introduced and defined by Fuller $et\ al.$ [11] which allow a more reliable interpolation.

Examples of our rates are shown in figures 2 and 3 using the pairs of nuclei (^{63}Co, ^{63}Ni) and (^{56}Fe,^{56}Co) as typical examples. The latter pair includes an even-even and odd-odd nucleus. The Q_β value for these nuclei is negative and in the laboratory ^{56}Co decays to ^{56}Fe by electron capture. To calculate the electron capture rate we have considered the 5 states in ^{56}Co below 1 MeV excitation energy and the lowest 1^+ state (at 1.72 MeV) explicitly, supplemented by the back-resonances.

The ^{56}Fe β decay rate can be calculated from the back-resonances due to the negative Q value.

The electron capture rates on both nuclei ^{63}Ni and ^{56}Co increase with temperature and density. Due to the negative Q_β value, electron capture is possible from all states in ^{56}Co and thus the increase with temperature is rather mild. However, in the case of ^{63}Ni electron capture is quite sensitive to temperature (at low densities), as it has to overcome a threshold of nearly 4 MeV which at the low densities ($\rho Y_e = 10^7$ and 10^{10} g/cm^3) is mainly achieved by thermal population of excited states in the parent nucleus, as the Fermi energies of the electrons (1.2 MeV and 2.4 MeV, respectively for $T_9 = 1$) is still noticeably smaller than the Q_β value of 3.67 MeV. However, at the higher densities electrons with energies above Q_β are sufficiently available to allow for efficient capture. In this case, the rate becomes only slightly dependent on temperature.

The ^{56}Fe β-decay rate shows a very steep temperature dependence and decreases with density. Both effects are readily explained. Due to the threshold of about 4.5 MeV, β decay is only possible from moderately excited states which have to be populated thermally leading to the strong temperature dependence. As the electron Fermi energy increases with density, an increasingly larger part of the phase space gets Pauli-blocked. Consequently the β-decay rate decreases with increasing density. Note that the centroid of the GT$_+$ strength distributions of the ^{56}Co ground state is at an excitation energy of around 8 MeV in ^{56}Fe. Thus at densities larger than $\rho Y_e = 10^9$ mol/cm^3 (corresponding to an electron Fermi
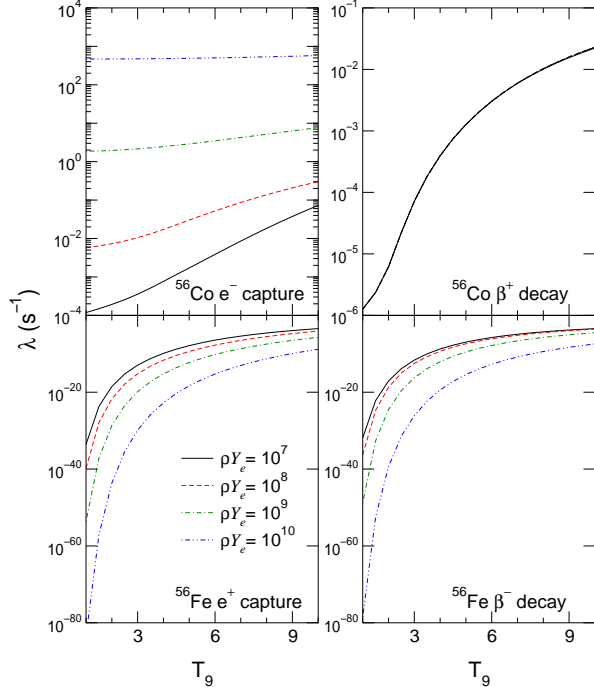
FIG. 2. Stellar weak interation rates for the pair of nuclei ^{56}Fe and ^{56}Co as a function of T_9 for selected values of ρY_e (in mol cm^{-3})

FIG. 3. Stellar weak interation rates for the pair of nuclei ^{63}Co and ^{63}Ni as a function of T_9 for selected values of ρY_e (in mol cm^{-3})

energy of about 5 MeV for $T_9 = 5$), the strong transitions associated with the centroid of the back-resonances are getting Pauli-blocked explaining the larger decrease with density even at high temperatures.

^{63}Co can β decay from all states and indeed already the ground state has a strong GT transition to the excited state in ^{63}Ni at 87 keV. Furthermore, the first excited state is at nearly 1 MeV excitation energy. Consequently, the ^{63}Co β-decay rate shows only a mild temperature dependence at low densities. Pauli-blocking by the electrons in the final state becomes, however, important at higher densities introducing effectively a threshold for the β decay which has to be overcome by thermal population of excited states in the parent. As a result, the rate develops an increasing sensitivity to temperature. The centroid of the GT$_+$ strength distribution of the ^{63}Ni ground state is at an excitation energy of around 2.5 MeV in ^{63}Co. Consequently Pauli blocking by electrons becomes increasingly important for densities above 10^9 g/cm^3.

The positron distribution does not play a role for the β^+ decay rate, which is virtually independent on density for both nuclei ^{63}Ni and ^{56}Co (this is already apparent from the FFN rates [9,10]). The ^{56}Co β^+ rate depends only mildly on temperature. This is different for ^{63}Ni where a threshold has to be overcome by thermal population in the parent. For both nuclei the β^+ decay rate is noticeably smaller than the electron capture rate which generally dominates the weak rates for charge-decreasing
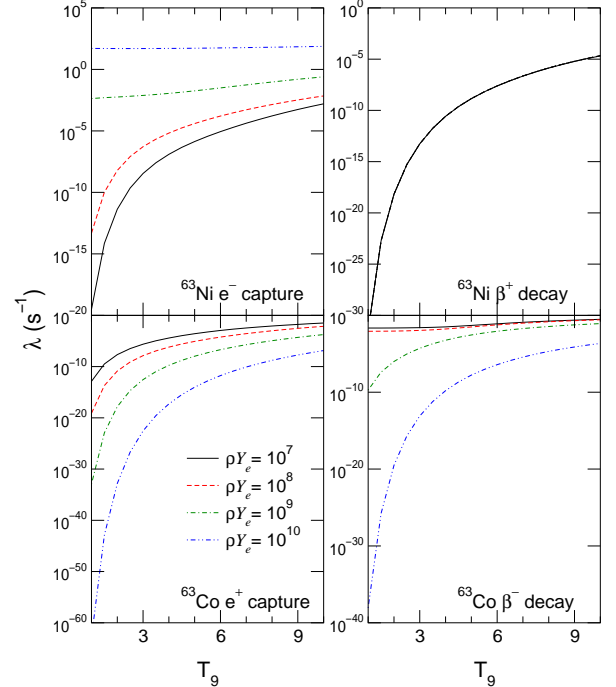
nuclear transitions under supernova conditions.

The positron capture rate decreases with density, but increases with temperature. Both dependencies are caused by the positron distribution where an increasing number of high-energy positrons gets available by raising the temperature or lowering the density. The latter is caused by the fact that the degeneracy parameter μ/kT is negative for positrons. Due to its threshold for positron capture, the rate on ^{56}Fe shows the steeper temperature dependence. Again, the positron capture rates are usually smaller than the competing β^- rates under supernova conditions for the nuclei of interest here.

The most interesting question clearly is: How do the shell model rates compare to the FFN rates?

To answer this question, we have calculated the ratio $\lambda_{\mathrm{FFN}}/\lambda_{\mathrm{SM}}$, where λ_{FFN} and λ_{SM} are the FFN and shell model rates, respectively. The FFN rates are taken from the electronic file available at [30]. For the comparison we choose 4 different temperature and density grid points $(T_9, \log(\rho Y_e))$: (3,7), (5,8), (5,9) and (10,10). Ratios for the two important weak processes, electron capture and β^- decay, are plotted in figures 4 and 5 for 4 different chains of isotones equally spanning the mass range between $A = 50\text{-}60$.

To understand the differences observed in figures 4 and 5 we have to recall how the FFN rates have been derived. At first, these authors considered experimental data for discrete transitions, whenever available (like we do in the present shell model rates). The main contribu-
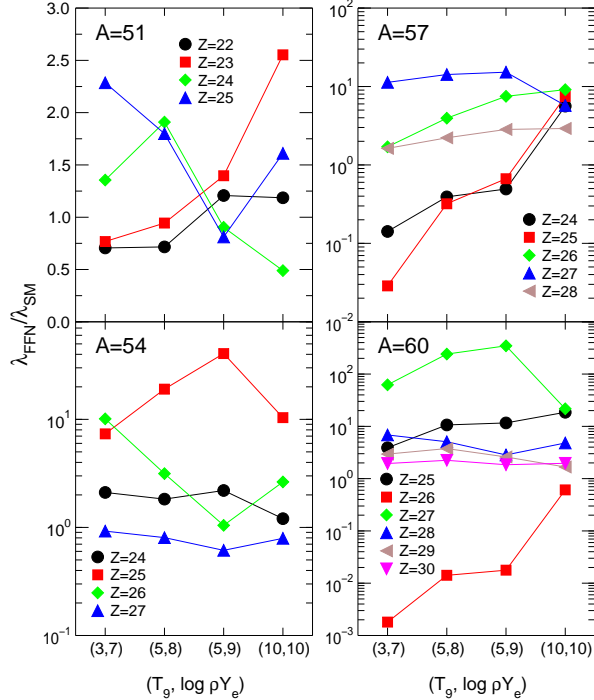
FIG. 4. Ratio of the FFN and shell model electron capture rates for nuclei in the mass chains $A = 51$, 54, 57, and 60 for selected values of temperature and density, T and density, $\log(\rho Y_e)$. The charge numbers refer to the parent nucleus.

FIG. 5. Ratio of the FFN and shell model β-decay rates for nuclei in the mass chains $A = 51$, 54, 57, and 60 for selected values of temperature T and density, $\log(\rho Y_e)$. The charge numbers refer to the daughter nuclei.

tion to the FFN rates usually comes from the so-called GT resonance which they parametrized on the basis of the independent particle model and which represents the total GT strength by a single state. Here it is not so important that the authors did not explicitly consider the quenching of the GT strength with respect to the independent particle model*. More relevant is where FFN placed the GT resonance. Here we will concentrate on the electron capture. The differences in the β^- decay rates follow then from a discussion of the back-resonance contributions.

FFN estimated the GT resonance energy E_{GTR} from 3 distinct contributions:

$$E_{GTR} = \Delta E_{sp} + \Delta E_{ph} + \Delta E_{pair}. \qquad (15)$$

The single particle term is calculated as follows. Starting with the independent particle model wave functions for the ground states of the parent and daughter nucleus, protons are acted on with the GT_+ operator leading to final neutron states, which, within the independent parti-

cle model, correspond to 1p-1h excitations of the ground state (or is the ground state). The corresponding excitation energy is readily calculated, where FFN used the single particle energies of Seeger [31]. If the GT_+ operation can lead to several different final states the excitation energy of the resonance is computed taking the weighted average of the different transitions. ΔE_{ph} is the particle-hole repulsion energy which has to be supplied to pull a neutron out of the daughter ground state. For simplicity, FFN put $\Delta E_{ph} = 2$ MeV for all nuclei. Finally, FFN argued that there is a penalty energy which has to be paid to break a neutron pair if there is an even number of neutrons in the daughter ground state. When applicable, this pairing energy is approximated by 2 MeV for all nuclei.

In previous publications [32] we have already pointed out that the shell model rates for important electron-capturing nuclei along the stellar trajectory (due to the ranking given in [28] these are generally odd-A and odd-odd nuclei) are usually smaller than the FFN rates. As one potential reason for this difference we have noted that the GT centroids for odd-A and odd-odd nuclei are usually at higher energies than assumed by FFN. We will discuss this difference and its potential origin in details below, but we note here that there are two other important ingredients (low lying transitions and Q_β values) which can lead to differences between the shell model

*The quenching in the GT_+ strength had not been established at the time FFN calculated the rates. In later discussions [11] these authors point to this effect and showed a way how to incorporate quenching effectively into the rates.
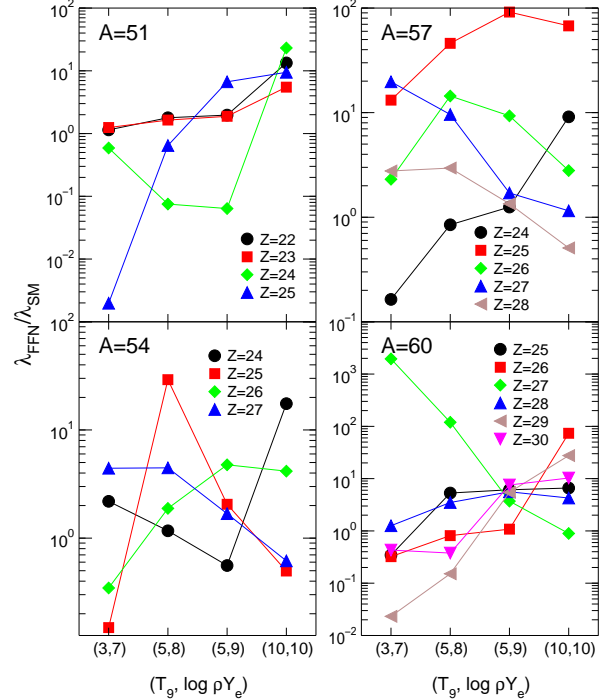
and FFN electron capture rates. In fact, for ^{51}Ti and ^{51}V we find from fig. 4 that the shell model rates are larger than the FFN rates at low temperature/density. For these cases the difference is due to the fact that the shell model predicts low-lying strength for the ground states (in ^{51}V to the second excited 5/2 state in ^{51}Ti, in ^{51}Ti to the lowest 1/2 state in ^{51}Sc) which are larger than the standard assignment ($\log ft = 5$) used in [8–10] for experimentally not known transitions. At larger temperatures/densities the low-lying strengths becomes less important as the capture proceeds mainly to the GT resonance; consequently the FFN rates are then larger than the shell model rates due to differences in the position of the centroid. (Note that the GT$_+$ strength distribution for ^{51}V has been measured and it agrees nicely with the shell model results [20].)

The nuclei ^{57}Mn and ^{60}Fe serve as examples for another source of differences between the shell model and FFN rates; the latter being noticeably smaller than the shell model rates at low temperatures/densities. This is due to the use of different Q_β values. FFN had to rely on the systematics available at the time, while modern compilations indicate that the Q_β values for these nuclei are about 950 keV (^{57}Mn) and 1.7 MeV (^{60}Fe) smaller than adopted by FFN. Obviously the too large Q value suppressed the electron capture at low temperatures/densities. With increasing temperature/density the electron Fermi energy grows strongly reducing the sensitivity to differences in the Q value.

More generally, one expects that the electron capture rates become less dependent on details of the GT strength distributions with increasing electron Fermi energies. This explains why the deviations between the FFN and shell model rates reduce with increasing temperature/density. In this limit, the FFN rates should be still slightly larger than the shell model rates due to the neglect of the quenching of the total GT strength in [8–10].

From the above discussion about the various contributions to the rates, one might distinguish 3 different temperature/density regimes along a stellar trajectory. At low (T, ρ) specific low-lying transitions can be quite important, supplementing the rate contribution from the GT resonance. This is particularly the case for electron capture, if the Q value only allows capture of high-energy electrons from the tail of the Fermi-Dirac distribution. At intermediate (T, ρ) the rates are usually dominated by the strong transitions involving the GT resonance. At high (T, ρ) (when E_e is large compared to Q_{ij} for transitions to the GT centroid) the rate becomes insensitive to the energy dependence of the GT distribution and hence the rate depends only on the total GT strength.

Differences between the shell model results and the FFN assumptions in the 3 ingredients (GT centroid energy, low-lying strength, Q values) lead also to differences in the β^- decay rates, as is shown in figure 5. Although the FFN β decay rates are usually somewhat larger than the shell model rates, no general picture emerges in this comparison, as the rates are usually given by the sum of low-lying transitions and contributions from the GT$_-$ distribution as well as of the back-resonances. As is discussed in [32] the misplacement of the GT$_+$ centroid effects the contribution of the back-resonances to the β-decay rates. In particular, the back-resonances in odd-odd parents (the GT$_+$ centroids of even-even nuclei have been often placed at too high energies by FFN) can be thermally excited more easily than assumed by FFN resulting in slightly larger β-decay rates for these nuclei. Examples are the odd-odd nuclei ^{60}Mn and ^{60}Cu. As FFN did not consider the quenching of the GT$_+$ strength, the contribution of the back-resonances is somewhat overestimated in FFN explaining the slightly larger FFN β-decay rates for ^{54}V or ^{54}Mn. Differences in the adopted Q-values effect mainly neutron-rich nuclei. An example here is the β-decay of ^{57}Cr, where FFN used the Q-value of 6.56 MeV rather than 5.60 MeV.

The pf-shell nuclei discussed here have not too extreme Y_e values and are therefore important at the earlier stages of the presupernova collapse involving low and intermediate (T, ρ) values. As in these regimes the energy position of the GT centroid plays an essential role, we will now investigate in details the differences between the placement of this centroid in the FFN compilation with the shell model rates (and the data).

In [32] we have pointed out that there are systematic differences between the placement of the GT centroid in the FFN compilations and the shell model results (and data, if available). It has been noted that the differences apparently depend on the pairing structure of the parent nucleus. For even-even parents, the GT$_+$ centroid is calculated at slightly smaller energies than assumed by FFN, while it has been noticed that for odd-A and odd-odd nuclei the centroid is at higher excitation energies than parametrized by FFN. The consequences for the electron capture and β-decay rates are obvious. If the kinematics is such that electron capture is dominated by transitions to the GT resonance, the FFN rates should be larger than the shell model rates as, for given temperature and density, less electrons are available to capture to the centroid if it resides at higher energies. This effect is strongest for odd-odd nuclei where the differences between the FFN and shell model rates can be larger than 2 orders of magnitude, i.e. for ^{60}Co (fig. 4) which is usually considered to be among the most effective electron-capturing nuclei along the collapse trajectory of a supernova.

Also for the β-decay rates the ratios systematically depend on the pairing structure of the parent. Here, however, the shell model rates are similar to the FFN rates for odd-odd parents (they are even often slightly larger), while they are smaller for odd-A and even-even nuclei. The reduction is usually largest for even-even nuclei.

The systematics assumed by FFN for the GT resonance energy in the daughter is most easily illustrated for parent nuclei with only $f_{7/2}$ protons and more than 28 neutrons (so that the $f_{7/2}$ orbital is blocked for GT$_+$

transitions). Then the single particle contribution to the GT resonance energy is about 1.8 MeV, if the neutron number is smaller $N \leq 32$, or 0, if $N > 32$. Thus one finds $E_{GTR} \approx 3.8$ (2.0) MeV for even-even parent nuclei and 5.8 (4.0) MeV for odd-odd parents. For odd-A parents one has $E_{GTR} = 3.8$ (2.0) MeV if the neutron number in the parent is even and 5.8 (4.0) MeV, if it is odd. Here the numbers in parentheses refer to parent nuclei with $N > 32$ for which the $p_{3/2}$ neutron orbitals are completely occupied.
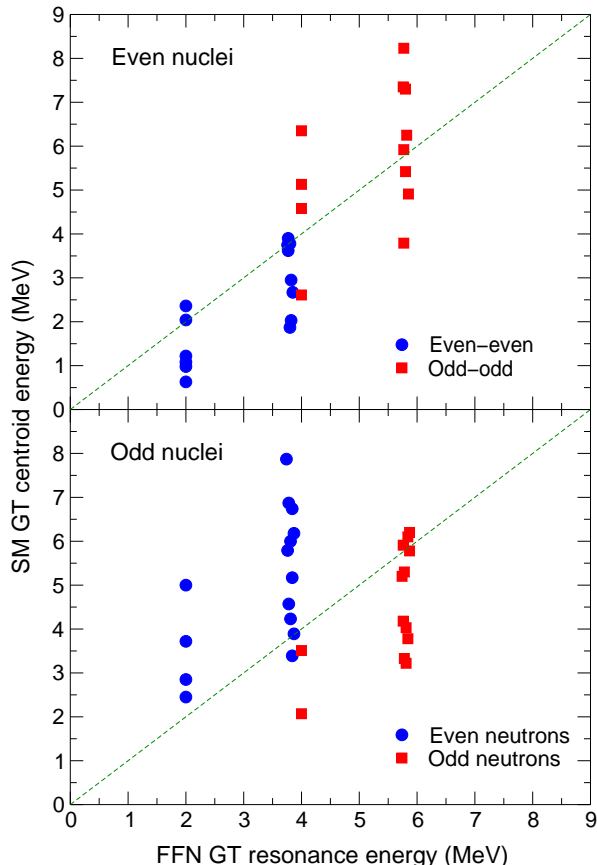
FIG. 6. Comparison of the FFN GT$_+$ resonance energies with the shell model centroid energies for various nuclei with $Z \leq 28$ and $N \geq 28$.

Figure 6 compares the shell model GT centroids with the FFN estimates of the GT resonance energy for about 45 nuclei with proton numbers $Z \leq 28$ for which the above given systematic of the FFN estimates apply. Indeed one clearly observes that the FFN GT resonance energies cluster around 2, 4, and 6 MeV. Clearly one expects that the shell model GT centroid energies are more scattered as the residual interaction fragments the GT strength and structure effects will also effect the GT distributions. But a more striking result is found if we compare the GT centroids for even-even, odd-A and odd-odd parent nuclei separately. Here we find that, compared to the shell model centroids, FFN places the GT reso-

nance energy usually at too high an energy for even-even parents and often at too low an energy for odd-odd parents. The situation is more interesting and also more telling for odd-A parents. Note that all those nuclei, for which FFN estimated the GT resonance energy by about 6 MeV, have parent nuclei with an odd number of neutrons and thus require an additional pairing energy in the FFN estimate. Compared to the shell model GT centroids the FFN estimates for these nuclei are too high. Then compare the nuclei with an even neutron number in the parent. They do not acquire the additional pairing energy in the FFN estimate. Compared to the shell model estimate, the FFN GT resonance energies are usually too low.

TABLE III. Comparison of the experimental centroids of the GT resonance with the FFN GT resonance energies and the shell model centroids. The data are from [33–37]. All energies are in MeV.

nucleus	data	FFN	shell model
^{54}Fe	3.7 ± 0.2	3.80	3.78
^{56}Fe	2.6 ± 0.2	3.78	2.60
^{58}Ni	3.6 ± 0.2	3.76	3.75
^{60}Ni	2.4 ± 0.3	2.00	2.88
^{62}Ni	1.3 ± 0.3	2.00	1.78
^{64}Ni	0.8 ± 0.3	2.00	0.50
^{51}V	4.8 ± 0.2	3.83	5.18
^{55}Mn	4.1 ± 0.3	3.79	4.57
^{59}Co	4.4 ± 0.3	2.00	5.05

Thus it is obvious from this comparison that there is a different dependence on the pairing structure of the parent ground state between the FFN assumptions and the shell model results. But, which is correct? Experimentally the GT$_+$ strength distribution has been studied for several even-even (^{54,56}Fe, ^{58,60,62,64}Ni) and 3 odd-A nuclei (^{51}V, ^{55}Mn, ^{59}Co) in this mass range. As pointed out in [38] the GT centroid for the even-even parents are generally at lower excitation energies in the daughter than for the odd-A nuclei. If the experimental centroids are compared to the FFN estimates one finds the same trend as discussed above for the comparison with the shell model centroids. Here we have calculated the experimental centroids from the measured GT distributions upto 8 MeV. For ^{62,64}Ni, however, we only consider the peak in the GT distribution corresponding to the GT resonance. The tail of the experimental distribution (see Fig. 1 in [20]), if real, is most likely due to states outside of our present model space. As demonstrated in Table III, the FFN GT resonance energy is usually at too high an energy for even-even parents, while it is at too low an energy for the 3 odd-A nuclei, investigated experimentally. We note, however, that these 3 nuclei all have an even neutron number in the parent and just do not allow to explore the assumptions which FFN made concerning the pairing energy contribution to the GT res-

onance energy. We stress that our shell model centroids are generally in good agreement with the data, as in fact the shell model calculations reproduce all measured GT_+ strength distributions quite satisfactory.

The differences in placement of the GT centroids explain the differences between the FFN and shell model weak interaction rates. As FFN assumes the GT resonance energy for odd-odd and odd-A parent nuclei with an even neutron number at lower energies than placed by the shell model, electron capture to these strong transitions is easier and hence the FFN electron capture rate is significantly larger than the shell model rate for these nuclei. For electron capture on even-even nuclei and for odd-A nuclei with an odd neutron number, FFN have generally placed the GT resonance energy at lower daughter energies than predicted by the shell model (or the data). This effect alone would make the FFN rates smaller than the shell model rates. However, it is largely compensated by the fact that FFN did not consider the quenching of the GT strength and by their consideration of experimentally known transitions at low excitation energies. Taken together, the FFN rates are also for these parent nuclei usually somewhat smaller than the shell model rates, with the notable exception of ^{56}Ni [18]. For reasons which will become apparent in the next section, the FFN rates on very neutron-rich odd-A nuclei with odd neutron number are also often smaller than the shell model rates.

Remembering the importance of the back-resonances for the β^- decay rates, the effect of the different placements of the GT centroid is obvious. In even-even nuclei and odd-A nuclei with even neutron number the shell model studies place the back-resonances at higher excitation energies than assumed by FFN. Correspondingly, its thermal population becomes less likely and hence the contribution of the back-resonances to the β^- decay rates decreases. On the contrary, experimental data and the shell model calculations indicate that the back-resonances reside actually at lower excitation energies in odd-odd nuclei than assumed by FFN. Consequently, the contribution of the back-resonances to the β^- decay rate of odd-odd parent nuclei should be larger than assumed in the FFN rates, which is indeed the fact for several nuclei like ^{54,56}Mn and ^{58}Co. The effect of the misplacement of the GT centroids on the β^- rates has already been discussed in [13,14,32].

In the next section we will argue why the systematics of the shell model GT centroids is correct. Furthermore, in connection with the well-established systematics of the GT centroids for the GT_- transitions, we will give a rather simple parametrization for these quantities. Although these arguments still have to be delivered, we will close this section pointing out that the present shell model rates are more reliable than the FFN ones and in fact should represent a fairly accurate description of the nuclear structure problem required to derive these rates. Then the weak interaction rates adopted in supernova simulations should be revised. We will speculate briefly

below about possible consequences which the shell model rates might have for the presupernova core collapse.

IV. SYSTEMATICS OF THE GT CENTROID ENERGIES

We begin our discussion by recalling that the systematics of the GT centroid energy E_{GT} is well understood for GT_- transitions. In fact, one finds in a very good approximation [39]

$$E_{GT} - E_{IAS} = a + b \cdot \frac{(N-Z)}{A}. \qquad (16)$$

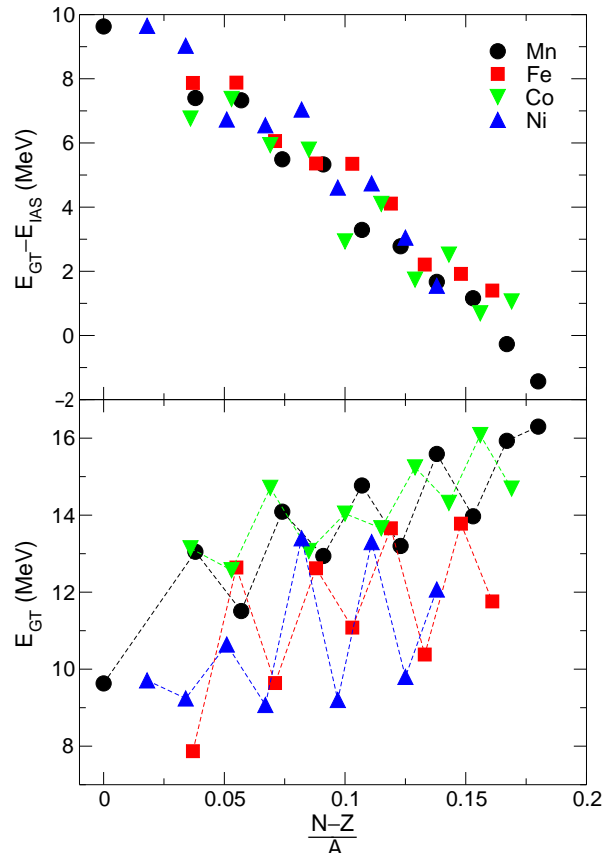The constants a, b can be derived by fit to measured GT_- strengths [39].

FIG. 7. The shell model GT_- centroid energy, relative to the energy of the isobaric analog state (upper panel) and to the daugther ground state (lower panel), for the Mn, Fe, Co, and Ni isotopes as function of $(N-Z)/A$. The pairing energy in the mass splitting between parent and daughter nuclei shifts the GT_- centroid energy for odd-A and odd-odd parents up in energy with respect to even-even parent nuclei.

In Fig. 7 we demonstrate that the centroids of our shell model GT_- strength distributions indeed exhibit this $(N-Z)/A$ dependence. Our results show a spread

of about 1 MeV which can be interpreted as the uncertainty introduced by nuclear structure effects. In passing we note that for nuclei with large neutron excess the GT$_-$ centroid energy can be below the IAS energy. As the figure is compiled for the isotope chains with $Z = 25-28$ it comprises all 3 different types of parent nuclei: even-even, odd-odd and odd-A. Clearly no systematic dependence on the pairing structure is found. Obviously such a dependence shows up if the GT centroid energies are plotted as measured relatively to the daughter ground state energy (lower panel of figure 7). It is trivially introduced by the differences in pairing energy between the various parent and daughter nuclei. As a consequence GT$_-$ centroids form now 3 distinguished bands: one for even-even nuclei, one for odd-A nuclei, and one for odd-odd nuclei the latter two shifted up in energy by about twice or four times the pairing energy, respectively.

As we will show now the same behavior is found for the centroids of the GT$_+$ strength distributions. Before we do so, however, it is useful to recall the origin of the $(N - Z)/A$ dependence of the GT$_-$ centroids. Here we will follow the nice discussion given by Bertsch and Esbensen [40]. Then the average excitation energy of the GT operator is given by

$$E_{GT} = \int_0^\infty dE \, ES(E) = \frac{\langle \boldsymbol{\sigma t}_\mp [H, \boldsymbol{\sigma t}_\pm] \rangle}{\langle \boldsymbol{\sigma t}_\mp \boldsymbol{\sigma t}_\pm \rangle} \qquad (17)$$

where the expression is valid for both GT$_-$ and GT$_+$ operators. Several pieces of the Hamiltonian do not commute with the GT operator. While the most of these contributions are cancelled in building the difference with the IAS energy, the $v_{\sigma\tau} \boldsymbol{\sigma}_1 \cdot \boldsymbol{\sigma}_2 \boldsymbol{\tau}_1 \cdot \boldsymbol{\tau}_2$ residual interaction gives rise to an energy shift that in the Tamm-Dancoff approximation is given by [40]

$$\Delta E_{\sigma\tau} = \frac{\langle v_{\sigma\tau} \rho \rangle 2 S_\beta}{3A} \qquad (18)$$

where $v_{\sigma\tau}\rho$ is the product of the integrated strength and the averaged ground state density. (In building the difference with the IAS energy a similar contribution arising from the $v_\tau \boldsymbol{\tau}_1 \cdot \boldsymbol{\tau}_2$ interaction has to be subtracted.) S_β is the total GT strength, which for the GT$_-$ operator and neutron-rich nuclei, can be approximated by the Ikeda sumrule, $S_{\beta-} = 3(N - Z)$. Upon substitution into (18), one finds the desired $(N - Z)/A$ dependence.

For the GT$_+$ operator one derives at the same expression for $\Delta E_{\sigma\tau}$, however, now considering $S_{\beta+}$. If one measures the GT$_+$ centroid from the parent ground state, the contribution from the other terms of the Hamiltonian are largely cancelled and one has upto a constant (reflecting for example the spin-orbit splitting) $E_{GT} = \text{const} + E_{\sigma\tau}$. The problem just reduces to find an appropriate parametrization of the total GT$_+$ strength. As has been pointed out in Ref. [38], the presently available data for pf shell nuclei suggest a scaling of the total GT$_+$ strength like

$$S_{\beta+} = a Z_v \cdot (20 - N_v) \qquad (19)$$

where Z_v, N_v are the number of valence protons and neutrons in the pf shell, respectively. This dependence corresponds to a generalized BCS model with pure proton and neutron pairing [41].
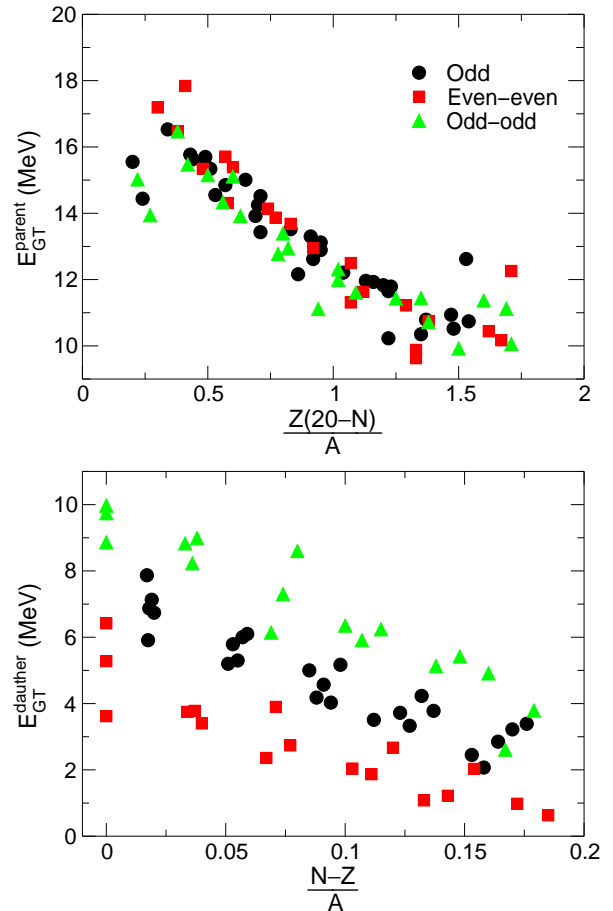

FIG. 8. Upper panel: shell model GT$_+$ centroid energy, relative to the parent ground state energy, for various nuclei in the mass range $A = 50 - 60$ as function of $Z_v(20 - N_v)/A$. Lower panel: shell model GT$_+$ centroid energy, relative to the daughter ground state energy, for the same nuclei as function of $(N - Z)/A$. The pairing energy in the mass splitting between parent and daughter nuclei shifts the GT$_+$ centroid energy for odd-A and odd-odd parents up in energy with respect to even-even parent nuclei.

We have calculated the GT$_+$ centroids for about 75 nuclei in the pf shell and if we plot these energies with respect to the parent ground state energies, they closely follow the $Z_v \cdot (20 - N_v)/A$ rule. Importantly, like for the case of the GT$_-$ centroids, no dependence on the pairing structure of the parent nucleus is observed. However, such a dependence, as we have seen above for the GT$_-$ centroids, is introduced if one measures the GT centroids with respect to the daughter ground state energies. This is again demonstrated in Fig. 8. Here we have chosen to plot the centroid energies as function of $(N - Z)$ which is the dominating dependence in the parent-daughter mass

splitting and is stronger than the $Z_v(20-N_v)$ dependence of $S_{\beta+}$. Like for GT$_-$, the centroids now group according to the pairing structure of the parent ground state. Again the centroids are lowest for even-even parents and the centroids for the odd-A and odd-odd parents are shifted up in energy by about 3 and 6 MeV, resp.

We note that the same pairing shifts of the $S_{\beta+}$ strength has already been suggested by Hansen in a general discussion of the β strength in nuclei [42].

The dependence of the GT$_+$ distribution on the proton and neutron number is nicely visualized in fig. 9 for the odd-$A = 61$ isotone chain. For comparison we note that the independent particle model, as assumed by FFN, places the GT$_+$ centroids at excitation energies of 4 MeV for ^{61}Fe and ^{61}Ni (the daughter nuclei have an even neutron number) and at 2 MeV for ^{61}Co. ^{61}Cu has 9 valence protons, thus allowing also for a $p_{3/2}$ proton being changed into a $p_{1/2}$ neutron. Relatedly, the GT$_+$ centroid is shifted slightly to 2.1 MeV. As has already been visible in fig. 6, the shell model shows quite a different dependence of the GT$_+$ distributions. At first, we observe that in all cases the strength is concentrated in an energy region of about 3-4 MeV width. Further, the centroid of this region decreases with increasing neutron excess. However, we stress that this decrease is basically due to the $(N-Z)$ dependence of the mass difference between parent and daughter nucleus, as the GT$_+$ centroid energy increases slightly with $(N-Z)$ if measured with respect to the parent ground state. The figure clearly shows no distinct dependence of the GT$_+$ centroid energy on the neutron pair configuration. We find the shell model centroids at excitation energies of 2.1 MeV (^{61}Fe), 3.7 MeV (^{61}Co), 4.7 MeV (^{61}Ni), and 6.7 MeV (^{61}Cu). Clearly the total GT$_+$ strength decreases with increasing neutron excess in the isotone chain due to the decreasing number of valence protons and the increasing Pauli blocking of the neutrons.

Finally we remark that the figure also shows that the thermal excitation of the strong backresonance transitions becomes easier with increasing neutron excess, as these transitions move to lower excitations energies.

V. CONCLUSIONS

Bethe and collaborators [7] had, more than two decades ago, focussed the attention on the importance played by the weak interaction in a supernova collapse. Subsequently about twenty years ago Fuller, Fowler and Newman (FFN) [8–10] outlined in their seminal work the theory to calculate stellar weak interaction rates. After this pioneering step the problem had been reduced to solve the related nuclear structure physics. While FFN understood the relevant physics correctly, due to lack of data and computational resources they were forced to estimate the relevant weak interaction rates on nuclei in the mass range $A = 45 - 60$ phenomenologically. Over the
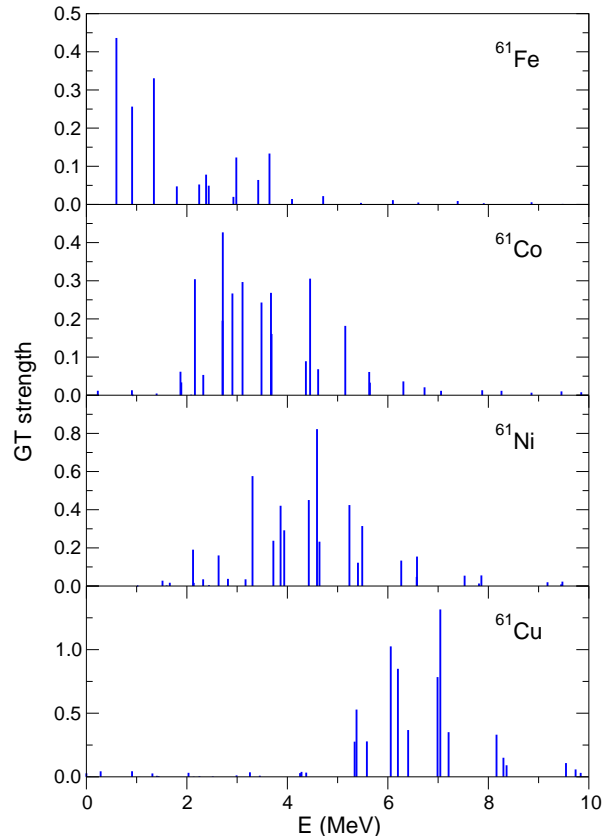

FIG. 9. The shell model GT$_+$ distributions for the odd $A = 61$ isotones as function of excitation energy in the daughter nucleus. Note the different scales used for the various nuclei.

years experimental findings about the fragmentation and positioning of the GT strength in these nuclei indicated the need for refinements of the rates and it became obvious [13,14] that the interacting shell model is the method of choice for this endeavour. First steps towards this goal have been undertaken using the shell model Monte Carlo technique [16], but it became clear that shell model diagonalization is the better suited tool to calculate reliable stellar rates. Impressive progress in both shell model programming (in particular due to the work by E. Caurier) and hardware development allows now for virtually converged calculations of the GT strength in pf shell nuclei, as they play a fundamental role during the presupernova collapse. In fact, Caurier et al. have demonstrated [20] that shell model diagonalization is able to reproduce all measured GT$_+$ and GT$_-$ strength distributions on nuclei around $A \approx 60$ and simultaneously describe the spectra and lifetimes of these nuclei also sufficiently well. As this is the relevant input to reliably calculate stellar weak interaction rates, it has been concluded that the shell model diagonalization approach of Ref. [20] has the necessary predictative power to calculate the rates. In this manuscript we have followed this conclusion and have

derived stellar weak interaction rates based on state-of-the-art shell model diagonalization. The calculation has been performed for more than 100 nuclei in the mass range $A = 45 - 65$ and covers the temperature and density regime expected in supernova physics. The rates have been compiled in a file using the same format as is customary for the FFN rates. The electronic version of the file can be received from the authors upon request. The files are also available in the effective rates formalism as derived in [11].

Differences between the shell model and the FFN rates are usually related to differences in the placement of the GT resonance energies. In analogy to the wellknown systematics of the GT_- centroid energies we have derived a similar systematics for the GT_+ resonance energies. In particular we have shown that the GT_+ centroid energies, if measured with respect to the parent ground state energy, are not dependent on the pairing structure of the parent nucleus. If the centroids are, however, measured with respect to the daughter ground state energy, the wellknown pairing energy contributions to the mass splitting between parent and daughter nuclei enters and the positions of the GT centroids are pushed up in energy for odd-A and odd-odd parents by twice and four-times the pairing energy, respectively. This systematic has not quite been considered in previous estimates of the weak interaction rates [9,10,28,43].
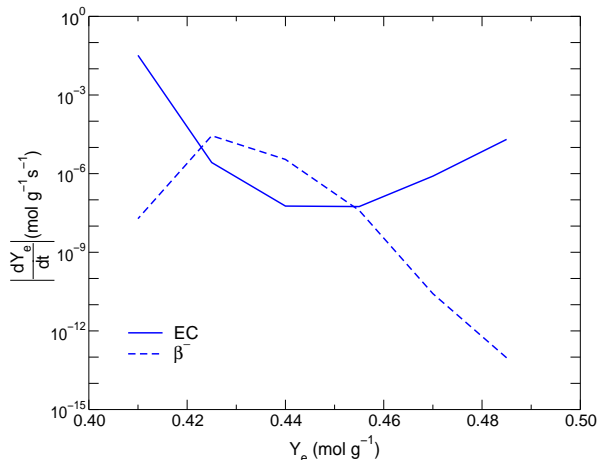

FIG. 10. Change in the total electron capture and β-decay rates as a function of electron-to-baryon ratio Y_e during a supernova collapse. The respective values for the temperature and density were taken from the stellar trajectory given in [28].

The shell model rates are usually smaller than the FFN rates. This is particularly the case for the electron capture rate on odd-odd nuclei and to a lesser extent on odd-A nuclei. This can be examplified for the nuclei ^{55}Co, ^{57}Co, ^{54}Mn, ^{60}Co and ^{58}Mn which the compilation of [28] subsequently ranks as the most effective electron capturing nuclei in the density regime $\rho = 10^7 - 10^{10}$

g/cm^3. For these nuclei the shell model rates are smaller than the FFN rates by factors 39, 12, 10, 346, and 19, respectively, where the comparison is made for those temperatures and densities where Ref. [28] lists the respective nucleus as most important. Already this comparison suggests that stellar electron capture rates are noticeably smaller than previously assumed. As speculated in [19], due to the smaller electron capture rates the core should radiate less energy away by neutrino emission, keeping the core on a trajectory with higher temperature and entropy.

Electron capture has to compete with β decay in the stellar environment. For even-even and odd-A nuclei, the shell model β-decay rates are generally also noticeably smaller than the FFN rates. But for odd-odd nuclei shell model and FFN rates are about the same. As the β decay of odd-odd nuclei is expected to contribute significantly to the total β decay rate during a collapse, the total β-decay rate should change less in supernova simulations than the electron capture rate, if the FFN compilation is replaced by the shell model results.

Obviously collapse calculations which use the shell model stellar weak interaction rates are desired and those studies are already initiated. Definite conclusions have to wait for the results of these simulations, but we can here update one interesting finding put forward in [44,32]. These authors argued that during the collapse the β decay rate will exceed the electron capture rate for a certain range of electron-to-baryon ratios Y_e. As a consequence the core can radiate energy away, (as the neutrinos can still leave the star without interaction) without lowering the Y_e value. This should have some interesting consequences for the size of the homologous core.

In [32] the regime in which the β-decay rate exceeds the electron capture rate has been estimated on the basis of shell model rates for a limited set of nuclei. Here we update this comparison by adopting the full set of shell model rates. To do so, we follow Ref. [44] and define the change of Y_e due to β decay (this increases the charge by one unit) and electron capture (which reduces the charge by one unit) as

$$\dot{Y}_e^{ec(\beta)} = \frac{dY_e^{ec(\beta)}}{dt} = -(+)\sum_k \frac{X_k}{A_k}\lambda_k^{ec(\beta)} \qquad (20)$$

where the sum runs over all nuclear species present in the core. and λ_k^{ec} and λ_k^{β} are the electron capture and β decay rates of nucleus k. The mass fraction is given by nuclear statistical equilibrium [28].

As in [32] we will follow the stellar trajectory as given in Ref. [44], although this is expected to change somewhat if the FFN rates are replaced by the shell model rates in the collapse simulation. Fig. 10 compares $\dot{Y}_e^{ec}$ and $\dot{Y}_e^{\beta}$ along the stellar trajectory where Y_e reduces here with time. Confirming the results of [32] the full set of shell model rates also reveals that the β decay rates are larger than the electron capture rates for

$Y_e = 0.42 - 0.455$. This might have important consequences for the core collapse possibly leading to cooler cores and larger Y_e values at the formation of the homologous core.

Thielemann and collaborators [45,6] have reported first attempts to explore the role of the shell model electron capture rates in type Ia supernovae. They find that the composition of the matter in the center is less neutron-rich than previously assumed. If the FFN rates are replaced by the shell model ones the overproduction of the neutron-rich Cr, Ti, and Fe isotopes which has been encountered in previous type Ia simulations with otherwise the same physics input [5], is removed. As the present shell model rates likely reduce the uncertainties related to the stellar electron capture rates, it is expected that type Ia simulations with the new shell model electron capture rates will serve as strict tests for the models and their parametrizations. Such comprehensive studies are in progress.

ACKNOWLEDGMENTS

[1] F. Hoyle, M.N.R.A.S. **106** 343
[2] D.D. Clayton, *Principles of Stellar Evolution and Nucleosynthesis* (Chicago Press, 1983)
[3] D. Arnett, *Supernovae and Nuclei* (Princeton University Press, 1996)
[4] P. Ruiz-Lapuente, R. Canal and J. Isern, *Thermonuclear Supernovae* (Kluwer Academic Publishers, Dordrecht, 1997)
[5] K. Iwamoto, F. Brachwitz *et al.*, Ap.J., in print
[6] F. Brachwitz, D.J. Dean, W.R. Hix, K. Iwamoto, N. Kishimoto, K. Langanke, G. Martínez-Pinedo, K. Nomoto, M.R. Strayer and F.-K. Thielemann, Ap. J., in print
[7] H.A. Bethe, G.E. Brown, J. Applegate and J.M. Lattimer, Nucl. Phys. A **324** (1979) 487
[8] G.M. Fuller, W.A. Fowler and M.J. Newman, ApJS **42** (1980) 447
[9] G.M. Fuller, W.A. Fowler and M.J. Newman, ApJS **48** (1982) 279
[10] G.M. Fuller, W.A. Fowler and M.J. Newman, ApJ **252** (1982) 715
[11] G.M. Fuller, W.A. Fowler and M.J. Newman, ApJ **293** (1985) 1
[12] M.B. Aufderheide, Nucl. Phys. A **526** (1991) 161
[13] M.B. Aufderheide, S.D. Bloom, D.A. Ressler and G.J. Mathews, Phys. Rev. C **47** (1993) 2961
[14] M.B. Aufderheide, S.D. Bloom, D.A. Ressler and G.J. Mathews, Phys. Rev. C **48** (1993) 1677
[15] C.W. Johnson, S.E. Koonin, G.H. Lang and W.E. Ormand, Phys. Rev. Lett. **69** (1992) 3157
[16] S.E. Koonin, D.J. Dean and K. Langanke, Phys. Rep. **278** (1996) 1
[17] D.J. Dean, K. Langanke, L. Chatterjee, P.B. Radha and M.R. Strayer, Phys. Rev. C **58** (1998) 536
[18] K. Langanke and G. Martínez Pinedo, Phys. Lett. B **436** (1998) 19
[19] K. Langanke and G. Martínez-Pinedo, Phys. Lett. B **453** (1999) 187
[20] E. Caurier, K. Langanke, G. Martínez-Pinedo and F. Nowacki, Nucl. Phys. A **653** (1999) 439.
[21] A. Poves and A.P. Zuker, Phys. Rep. **70** (1981) 235
[22] I.S. Towner and J.C. Hardy, in *Symmetries and Fundamental Interactions in Nuclei*, eds. W.C. Haxton and E.M. Henley (World Scientific, Singapore, 1995) p.183.
[23] A. R. Edmons, *Angular momentum in Quantum Mechanics* (Princeton University Press, Princeton, New Jersey, 1960)
[24] F. Osterfeld, Rev. Mod. Phys. **64** (1992) 491.
[25] B. A. Brown and B H. Wildenthal, At. Data Nucl. Data Tables **33** (1985) 347.
[26] K. Langanke, D. J. Dean, P. B. Radha, Y. Alhassid, and S. E. Koonin, Phys. Rev. C **52** (1995) 718.
[27] G. Martínez-Pinedo, A. Poves, E. Caurier, and A. P. Zuker, Phys. Rev. C **53** (1996) R2602.
[28] M.B. Aufderheide, I. Fushiki, S.E. Woosley and D.H. Hartmann, Ap.J.S. **91** (1994) 389
[29] D.L. Tubbs and S.E. Koonin, Ap.J.Lett. **232** (1979) L59
[30] http://ie.lbl.gov/astro/fuller.html
[31] P.A. Seeger and W.M. Howard, Nucl. Phys. A **238** (1975) 491
[32] G. Martínez-Pinedo, K. Langanke and D.J. Dean, Ap. J. in print.
[33] W.P. Alford, R.L. Helmer, R. Abegg, A. Celler, D. Frekers, P. Green, O. Haeusser, K. Henderson, K. Hicks, K.P. Jackson, R. Jeppesen, C.A. Miller, A. Trudel, M. Vetterli, S. Yen, H. Pourang, J. Watson, B.A. Brown and J. Engel, Nucl. Phys. A **514** (1990) 49.
[34] M.C. Vetterli, O. Haeusser, R. Abegg, W.P. Alford, A. Celler, D. Frekers, R. Helmer, R. Henderson, K.H. Hicks, K.P. Jackson, R.G. Jeppesen, C.A. Miller, K. Raywood and S. Yen, Phys. Rev. C **40** (1989) 559.
[35] S. El-Kateb, K.P. Jackson, W.P. Alford, R. Abegg, R.E. Azuma, B.A. Brown, A. Celler, D. Frekers, O. Haeusser, R. Helmer, R.S. Henderson, K.H. Hicks, R. Jeppesen, J.D. King, K. Raywood, G.G. Shute, B.M. Spicer, A. Trudel, M. Vetterli and S. Yen, Phys. Rev. C **49** (1994) 3128.
[36] W.P. Alford, B.A. Brown, S. Burzynski, A. Celler, D. Frekers, R. Helmer, R. Henderson, K.P. Jackson, K. Lee,

A. Rahav, A. Trudel and M.C. Vetterli, Phys. Rev. C **48** (1993) 2818.

[37] A.L. Williams, W.P. Alford, E. Brash, B.A. Brown, S. Burzynski, H.T. Fortune, O. Haeusser, R. Helmer, R. Henderson, P.P. Hui, K.P. Jackson, B. Larson, M.G. McKinzie, D.A. Smith, A. Trudel and M. Vetterli, Phys. Rev. C **51** (1995) 1144

[38] S.E. Koonin and K. Langanke, Phys. Lett. B **326** (1994) 5

[39] K. Nakayama, A.P. Galeao and F. Krmpotic, Phys. Lett. B **114** (1982) 217

[40] G.F. Bertsch and H. Esbensen, Rep. Prog. Phys. **50** (1987) 607

[41] J. Engel, S. Pittel, M. Stoitsov, P.Vogel and J. Dukelsky, Phys. Rev. C **55** (1997) 1781

[42] P.G. Hansen, Advances in Nuclear Physics, eds. M. Baranger and E. Vogt, vol. 7 (1973)

[43] F.K. Sutaria and A. Ray, Phys. Rev. C **52** (1995) 3460

[44] M.B. Aufderheide, S.D. Bloom, G.J. Mathews and D.A. Resler, Phys. Rev. C **53** (1996) 3139

[45] F.-K. Thielemann, F. Brachwitz, D.J. Dean, C. Freiburghaus, W.R. Hix, K. Iwamoto, K.-L. Kratz, K. Langanke, G. Martínez-Pinedo, K. Nomoto, B. Pfeiffer and M.R. Strayer, *Proceedings of the Strassburg workshop on double-beta decay rates*, (Strassburg, march 1999), to be published